Journal of Environmental Chemical Engineering 14 (2026) 121283

Contents lists available at ScienceDirect

Journal of Environmental Chemical Engineering

journal homepage: www.elsevier.com/locate/jece

Industrial assessment of recycled steelmaking slag as a sustainable alternative to carbon black in NBR composites

Anna Gobetti [a,*], Giovanna Cornacchia [a], Silvia Agnelli [a], Candida Petrogalli [a], Mattia Ramini [b], Mario Costardi [b], Roman Christopher Kerschbaumer [c], Maurício Azevedo [c], Giorgio Ramorino [a]

[a] Department of Mechanical and Industrial Engineering, University of Brescia, Via Branze 38, Brescia 25123, Italy
[b] Italian Gasket S.P.A., Via Tengattini N.9, (Bs), Paratico 25030, Italy
[c] Polymer Competence Center Leoben GmbH, Sauraugasse, 1, Leoben 8700, Austria

ARTICLE INFO

Keywords:
Electric arc furnace slag as filler
Injection molding, filled NBR, sustainable rubber compounds, cure kinetic
Carbon black replacement

ABSTRACT

This research assesses the industrial viability of black slag from electric arc furnace (EAF) as an eco-friendlier alternative to carbon black (CB) in nitrile butadiene rubber (NBR) formulations for technical components. Three compounds, at equal filler volume fraction, were prepared: a conventional CB-filled NBR, a fully slag-filled version, and a partial substitution (50 % slag and 50 % carbon black). Rheometric analysis showed that replacing CB with slag does not affect vulcanization kinetics, temperature dependence or activation energy; only the maximum torque (MH) and thus cured-rubber mechanical properties varied. Adding slag slightly lowers material viscosity (reduced minimum torque, ML). Injection molding of O-rings encountered filling problems: coarse slag particles (≤100 μm) blocked narrow mold gates (≈50 μm). By contrast, compression molding of flat plates encountered no processing issues. Mechanical tests revealed that tensile and tear strengths progressively decrease as slag content rises, driven by the slag angular shape and particle size. Tribological trials indicated that while friction coefficients drop with more slag, wear rates increase. ATR-FTIR spectra confirmed that slag does not alter the NBR's molecular structure, and thermal conductivity and glass transition temperature (≈–25.5 °C) remain unchanged. Notably, slag inclusion enhances thermal degradation resistance. Overall, the 50 % slag formulation strikes the best balance between environmental impact and performance, offering substantial eco-benefits with moderate loss of mechanical strength. Future work should target improved slag size and shape and/or alternative moulding techniques, such as injection-compression, to fully leverage EAF slag's potential as a sustainable, drop-in filler in high-performance elastomers.

1. Introduction

The rubber industry relies heavily on fillers to enhance the properties of rubber compounds in order to improve or modify technological properties, processability or to reduce costs and environmental impact. Among reinforcing fillers, carbon black ranks among the most commonly employed in rubber applications due to its ability to significantly improve mechanical properties. On the other hand, the production of carbon black raises environmental concerns, as it is a petroleum-derived reinforcing filler with a considerable carbon footprint, making it a critical sustainability challenge for the rubber industry. In particular, it has been estimated that the emissions associated with carbon black production are in the range of 1.5–3.5 kg CO_2eq/kg [1](for comparison, the production of 1 kg of steel using only scrap-based EAF operation implies the emission of about 0.4 kg CO_2eq [2]).

Steel manufacturing from ferrous scrap utilises the EAF method, resulting in black slag as the primary by-product. EAF slag cannot be avoided because it is a byproduct essential to the production of steel: it protects the furnace refractories and contributes to the removal of undesired elements, such as phosphorus and sulphur [3]. The management of slag presents both environmental and economic challenges, especially considering that in Europe, the annual production of steel by EAF route

* Corresponding author.
E-mail addresses: anna.gobetti@unibs.it (A. Gobetti), giovanna.cornacchia@unibs.it (G. Cornacchia), silvia.agnelli@unibs.it (S. Agnelli), candida.petrogalli@unibs.it (C. Petrogalli), mattia.ramini@italiangasket.com (M. Ramini), mario.costardi@italiangasket.com (M. Costardi), roman.kerschbaumer@pccl.at (R.C. Kerschbaumer), mauricio.azevedo@pccl.at (M. Azevedo), giorgio.ramorino@unibs.it (G. Ramorino).

https://doi.org/10.1016/j.jece.2026.121283
Received 21 November 2025; Received in revised form 5 January 2026; Accepted 16 January 2026
Available online 17 January 2026

is approximately 60 million tons [4]. EAF slag accounts for about 10–15 % of the produced steel, so that the annual European slag production is about 6–9 million tons [4]. EAF slag's chemical and physical characteristics are determined by the production technique, the scrap feedstock, and the desired steel specification. It mainly consists of iron, calcium and silicon oxides, along with other oxides in minor quantities. The mineralogy is similar to that of volcanic rocks, being prevalently constituted of crystalline phases such as calcium silicates (larnite and bredigite), calcium alumino-ferrites (brownmillerite) and calcium aluminates (mayenite) [5]. Despite having potentially valuable properties, exploited mainly in the civil engineering sector as artificial aggregate, a substantial portion of this material is still disposed of in landfills, consuming valuable land resources and posing potential environmental risks due to the possible leaching of heavy metals over time. The primary challenges associated with slag reuse stem largely from its variable chemical composition, the leaching of heavy metals, and the uncertain regulatory context. In recent decades, steel manufacturers have made significant investments in the development of advanced production processes with the objective of reducing slag leaching. However, concerns regarding heavy metal leaching persist among users and regulators, thereby impeding the effective valorization of slag.

A non-conventional application of slag that can overcome environmental concerns is its uses as filler in polymer compounds, as it allows the inertization of the slag, preventing its possible heavy metals leaching. It is important to note that Life Cycle Assessment studies have demonstrated that the process which exerts the most significant environmental impact in relation to the disposal of slag in landfills is inertization with cement [6]. In this particular application, the polymer matrix itself inertizes the slag, immobilizing any heavy metals and eliminating the need for cement-based treatments at the terminal stage of its life cycle [7].

Recent years have seen a surge in investigations into using electric steelmaking by-products as agents in a variety of polymer matrices. Research has shown its effective incorporation into rubber compounds, where it serves as a sustainable alternative to conventional fillers [6,8]. Studies have also demonstrated that EAF slag can serve as a viable replacement for carbon black in rubber composites, delivering comparable performance with a reduced environmental impact [9] among other investigated waste as rice husk ash, peanut shell powder, waste wood, etc. [10–14]

The valorization of industrial byproducts as functional fillers in elastomeric compounds addresses dual environmental concerns: reducing petroleum-derived material consumption while simultaneously diverting industrial waste from disposal. Previous research has established that EAF slag possesses physical and chemical properties that could enable its application as non-conventional filler in rubber compounds. However, the feasibility of implementing such materials in industrial applications requires a comprehensive evaluation beyond basic characterization.

This paper extends previous findings on the viability of EAF slag as a carbon black replacement [9] in NBR compounds by focusing specifically on industrial processability and application-specific properties relevant to real applications. While earlier studies demonstrated that partial replacement of carbon black with EAF slag (particularly at 50 % substitution levels) shows promising results in terms of basic mechanical properties, this research investigates whether such compounds can meet the demanding requirements of industrial processing methods and functional performance in real-world sealing applications.

The principal goal of this investigation is to determine whether NBR compounds containing EAF slag as a partial or complete replacement for carbon black can be effectively used in sealing applications, therefore key physicochemical and tribological properties that directly influence sealing performance, including thermal stability, surface characteristics, and wear behaviour are examined. Moreover, the possibility to process them by using industrial manufacturing techniques, particularly injection moulding, which represents a common production method for technical components, is investigated.

By transitioning from laboratory-scale feasibility to industrial-scale integration, this research has the goal of merging theoretical sustainability improvements and practical application. The findings provide crucial insights for rubber manufacturers seeking to incorporate more sustainable materials into their formulations while maintaining the performance standards required for critical applications such as fluid sealing components.

2. Materials and methods

2.1. Materials

For this study, Ligom Spa (BG, Italy) supplied the rubber formulations. The base polymer was a sulfur-cured nitrile butadiene elastomer, reinforced with either carbon black, electric steelmaking by-product, or a hybrid blend of the two.

The formulations were reinforced with N772-grade semi-reinforcing furnace carbon black (density 1.8 g/cm^3). The electric steelmaking by-product, supplied by ASONEXT SPA (BS, Italy) and derived from carbon steel production, was pulverized to below 100 μm and exhibited a density of 4.1 ± 0.2 g/cm^3 —approximately twice that of the carbon black. This slag particle size was intentionally selected as an industrially realistic compromise between grinding effort and composite performance.

Maintaining a constant total filler volume, three compounds were prepared: NBR 0 % slag (100 vol% carbon black), NBR 100 % slag (100 vol% EAF slag) and NBR 50 % slag (50 vol% of each). Selection was guided by micromechanical theories that link reinforcement directly to filler volume fraction. Given the significant density disparity between fillers, weight-based formulations were avoided to eliminate confounding factors. The selection of 0 %, 50 %, and 100 % slag substitution levels was designed to evaluate the full range of replacement possibilities at constant filler volume fraction, rather than to optimize slag loading for maximum performance. This approach provides fundamental understanding of slag effects that can guide future formulation optimization for specific applications. The detailed recipes are provided in Table 1.

Compounding was carried out in a closed mixer at 30 rpm: the polymer and additives were blended for 30 s before the fillers were introduced. The batch was then discharged at 135 °C, allowed to cool, and sheeted on an open mill together with sulfur and accelerators. Final curing was performed in a compression mold at 160 °C for 20 min.

2.2. EAF Slag characterization

XRF spectroscopy was employed to determine the chemical composition of the EAF slag. Mineral phases were then identified via SEM–EDXS analysis of polished samples to separate and classify each

Table 1
Recipe of tested compounds.

Components		NBR 100 % Slag	NBR 50 % Slag	NBR 0 % Slag
NBR	[phr]		**100.00**	
ZnO	[phr]		**5.00**	
Stearic acid	[phr]		**0.50**	
Antioxidants	[phr]		**1.00**	
Plasticizers	[phr]		**16.30**	
Sulphur	[phr]		**0.40**	
Accelerators	[phr]		**1.00**	
Total Filler	[phr]	**132**	**96**	**60**
	[%v/v]	21	21	21
Detail: Filler composition				
Carbon black	*[phr]*	*0*	***30***	***60***
	[%v/v]	*0*	*10.5*	*21*
EAF slag	*[phr]*	***132***	***66***	*0*
	[%v/v]	*21*	*10.5*	*0*

phase. In addition, standardized leaching tests—conducted on both the slag particles and the composite materials at different granulometries—were used to investigate how the polymer matrix reduces metal release. For further details pertaining to the characterisation of the slag used in this study, please refer to [9].

2.3. Compound Characterization

2.3.1. Processability

The impact of EAF slag on processing characteristics is examined through curing kinetics and the activation energy of the vulcanization reaction, the viscosity of compounds and from injection moulding trials at industrial laboratory scale.

2.3.1.1. Crosslink kinetic. In order to determine crosslinking kinetics, rheometric tests were carried out by a Moving Die Rheometer (MDR 2000) from Alpha Technologies (Hudson, Ohio, United States) in accordance with ASTM D5289 [5]. Rheometric tests were performed at different temperatures, namely 165°C, 177°C, 185°C, 195°C and 200°C, for 12 min, using a frequency of 1.7 Hz and an oscillation amplitude of 3°.

By normalizing the rheometric traces according to Eq. 1, the degree of crosslinking (α %) is calculated.

$$\alpha[\%] = \frac{M_i - M_L}{M_H - M_L} \quad (1)$$

M_i represents the torque measured at time i; M_L and M_H denote the lowest and highest torque values, corresponding to the fully uncrosslinked (0 %) and fully crosslinked (100 %) states.

Assuming a first-order reaction (n = 1), the curing kinetics can be described by the Eq. 1[15]:

$$\frac{d\alpha}{dt} = k(1-\alpha) \quad (2)$$

By readjusting this equation and integrating both sides, it is possible to obtain (for $t_{s1} \leq t \leq t_{90}$) Eq. 3.

$$\ln[1-\alpha(t)] = -\,k\,(t - t_{s1}) \quad (3)$$

where t_{s1} is the scorch time and t_{90} corresponds to the time when the torque achieves 90 % of the maximum level (usually associated with 90 % od curing).

By plotting $\ln[1-\alpha(t)]$ vs $(t - t_{s1})$, a curve with a linear portion is obtained. From the linear fitting of the part of the plot exhibiting linear behavior, the apparent cure rate constant (k) at each isothermal temperature was obtained.

The temperature dependence of the rate parameter was analysed according to the Arrhenius law (Eq. 4):

$$k = Ae^{\frac{E_a}{RT}} \quad (4)$$

where A denotes the pre-exponential coefficient, Ea is the apparent activation energy, R stands for the ideal gas constant, and T represents the absolute temperature in kelvins. A plot of ln k versus 1000/T was constructed for the five test temperatures, and E_a was extracted from the slope $-E_a/R$ by linear regression.

2.3.1.2. Viscosity. The compounds' rheological behavior was analyzed using an RPA at 160 °C via frequency sweep tests in oscillatory mode (angular frequency ω ranging from 300 to 6 rad/s, corresponding to 47.75–0.995 Hz). An amplitude sweep of 0.1° was applied. Prior to testing, samples were conditioned by preheating for 4 min. Viscosity measurements were carried out under two protocols: one without preshearing during preheating (0.201° amplitude, f = 0.5 Hz) and one with preshearing (3° amplitude, f = 5 Hz).

2.3.1.3. Injection moulding trials (C_p e shear heating). Processing behavior of the compound was evaluated through injection moulding trials conducted at both laboratory and industrial scales, thanks to the technical support provided by Italian Gasket Spa (Paratico, BS, Italy).

A horizontal 190 Ton MIR injection moulding machine was used, with reciprocating screw, length over diameter ratio (L/D) of about 16. The machine is equipped with a mould with a single nozzle injection system and 174 cavities, used to produce O-rings (internal diameter: 13 mm; section diameter: 2 mm). It is important to emphasize that this is a full-scale industrial mould, not a pilot or low-cavity prototype, as the goal of the experiment was to realistically assess the compounds rheological behaviour under standard production conditions. The O-ring gasket type was chosen because it is the simplest geometry available in the company to understand the processing behaviour of rubber compounds.

Table 2 reports details of the processing conditions implemented for the injection moulding. The first trial was carried out on NBR 0 % slag compound, and the process parameters setup was 120 bar of injection pressure, 80 % of injection speed, 20 rpm of screw speed rotation, 65°C of barrel temperature, 190°C of both fixed and movable plate temperature and 85 s of curing time. Such parameters were selected on the basis of the company experience with NBR compounds, with the used injection moulding machine and mould, to get the best trade-off between productivity and performance.

Subsequently, NBR 50 % slag and finally NBR 100 % slag were injection moulded. In both cases, as the injection time increased too much, the parameters were adjusted, and, in particular, injection pressure and injection speed were increased to the final values reported in Table 2. Despite these modifications, the processing conditions cannot yet be considered optimized for full-scale production. Nevertheless, it was possible to produce sample parts, although further process optimization would be required to achieve ideal manufacturing conditions. Further results and comments are reported in the Results session.

To enable a rational analysis of the injection moulding process, the temperature at the rubber's nozzle exit (T_{SH}) was measured using an infrared thermal camera (Diacam C.A 1882, Chauvin Arnoux Group, Asnières-sur-Seine, France), featuring an accuracy of ±2 °C and a thermal resolution of 0.08 °C. An emissivity value of 0.95 was applied for the rubber, according to the device's material settings.

2.3.2. Physicochemical characterization

2.3.2.1. Density. Density of rubber cured materials was measured according to ASTM D297–15 standard [16].

2.3.2.2. Thermal conductivity. A sample (50 mm diameter and 2 mm thickness) is positioned between the heated top plate and the cooled bottom plate of a guarded heat flow meter DTC-300, supplied by TA Instruments (New Castle, Delaware, United States). This device operates under steady-state conditions and measures the heat transfer through the specimen via a heat flux transducer. Due to the low thermal conductivity of rubber compounds, a sample thickness of 2 mm was selected to ensure accurate measurements. Considering the limited heat transfer capability of rubber compounds (0.15 – 0.4 W/mK [17]). A pneumatic

Table 2
Operating Conditions Applied During Injection Moulding Tests.

Process parameter		NBR 0 % Slag	NBR 50 % Slag	NBR 100 % Slag
Injection Pressure	[bar]	120	125	140
Injection Speed	[%]	80	90	95
Screw Speed Rotation	[rpm]	20	20	20
Barrel Temperature	[°C]	65	65	65
Fixed and movable plates temperature	[°C]	190	180	180
Injection Time	[s]	5	15	30
Curing time	[s]	85	85	85

load of 0.16 MPa is applied to minimize contact resistance. Through the measurement, a temperature gradient (ΔT) is established as the heat is transferred originating at the upper heated plate, through the sample, to the lower cooled ones. Once thermal equilibrium is achieved, the heat flow rate (Q̇) is recorded. Using the Fourier's law, as expressed in Eq. 5, the thermal conductivity (λ) is determinated.

$$\lambda = \frac{\dot{Q}d}{A\Delta T} \tag{5}$$

Where A is the specimen area and d its thickness. The heat flow measurement performed in compliance to standard ASTM E1530 [18]. Thermal conductivity at 35 °C was measured on one sample taken from each crosslinked NBR test plate.

2.3.2.3. ATR/FTIR. An ALPHA II FT-IR spectrometer (Bruker Italy Srl), fitted with a germanium ATR crystal, was employed to perform Attenuated Total Reflection-Fourier Transform Infrared (ATR-FTIR) spectroscopy. The ATR sampling technique introduces IR light through a crystal that interacts with the pressed sample surface.

Measurements were conducted at a resolution of 4 cm^{-1} , applying 24 scans across a spectral range of 400–4000 cm^{-1} . After baseline correction, spectra were obtained as absorbance versus wavenumber (cm^{-1}) for qualitative identification of the main functional groups.

2.3.2.4. Thermogravimetric analysis (TGA). Thermogravimetric measurements were carried out using a TA Instruments Q500 analyzer. Approximately 10 mg of each specimen was placed in a platinum crucible and subjected to a nitrogen flow while being heated from room temperature to 560 °C at 10 °C·min^{-1} . After the mass stabilized, the material was held at 300 °C for 2 min, then switched to an oxygen atmosphere and ramped up to 800 °C at the same heating rate to determine the carbon black and ash contents.

2.3.2.5. Differential scanning calorimetry (DSC). The DSC analysis allowed to identify the glass transition temperature. The DSC scans were conducted under a inert atmosphere (N_2) and the temperature span from –90°C up to 80°C, by a Q100 DSC instrument from TA Instruments. The procedure begins with cooling the samples from room temperature to –90°C at a rate of 10°C per minute, followed by maintaining them at –90°C for one hour, and then heating them back to room temperature at the same rate of 10°C per minute while collecting thermal data.

To calculate the shear heating parameter from the shear heating temperature, useful to analyse the injection moulding trials, the specific heat capacity (C_p) at the T_{SH} is needed. Therefore, C_p was measured by DSC measurements according to ASTM E1269–11 standard. A DSC Star System DSC1/700 by Mettler Toledo (City, State, Cuuntry) was used, heating from 45°C to 200°C at 20 °C/min, in nitrogen atmosphere, using a synthetic sapphire as a heat flow calibration standard.

2.3.3. Mechanical characterization

2.3.3.1. Tear strength. Tear strength measurements were conducted according to ASTM D 624 B standard method. Results were recorded in newtons per millimeter (N/mm) [19].

2.3.3.2. Tribological behaviour. Rubber samples were tested on a THT pin-on-disc tribometer to quantify material loss under sliding contact. A 5 mm-diameter, flat-ended pin made of 100Cr6 steel served as the counterface, rubbing against a 50 mm-diameter, 2 mm-thick rubber disc. All trials took place at ambient temperature, with a constant normal force of 5 N and a sliding velocity of 80 mm/s, until the pin had covered a total of 200 m. When operated in a single-direction mode, the wear scar's diameter was 5 mm; switching to a back-and-forth (reciprocating) motion produced a 13 mm-wide track. Throughout each run, the friction coefficient (COF) was recorded with respect to distance: after an initial spike, it settled into a steady plateau, which was recorded as the equilibrium COF. Finally, the specific wear rate WsW_sWs (expressed in g/(N·m)) was derived from the sample's mass loss (initial minus final mass), the applied load PPP, and the total sliding distance lll, using the formula reported in Eq. 6.

$$W_s = \frac{(\Delta m)}{Pl} \tag{6}$$

Finally, the wear mechanisms were studied by SEM LEO EVO 40 VPS equipped by EDS probe.

3. Results

3.1. EAF Slag characterization

The detailed results of EAF slag characterization are shown already in [9], and here a summary is reported. The ternary diagram presented in Fig. 1 illustrates the chemical composition obtained via XRF, focusing on CaO + MgO, SiO_2 + Al_2O_3, and FeOn + MnO [wt%]. The highlighted region represents the typical compositional range for EAF slag used as filler, based on data from the REACH Ferrous Slag Consortium. The studied slag composition falls within this standard range, confirming its representativeness for industrial applications. The basicity index (BI4) of the slag was determined to be 2.3, which is within the range that promotes the formation of unstable spinel phases, such as brownmillerite, affecting the leachability of chromium, as confirmed by subsequent leaching tests.

The morphology of the slag particles is highly irregular, with angular and rough surfaces. Fig. 2 shows the transversal micrograph of EAF slag-filled NBR specimens by SEM analysis. The specimens were broken in liquid nitrogen in order to observe the morphology and dimensions and distribution of the incorporated slag particles.

Even though the material was sieved to a nominal size under 100 μm, a significant portion of the particles remains under the average diameter of 50 μm as highlighted by the granulometric distribution reported in Fig. 3 [9].

The mineralogic phase identification where obtained by SEM integrated with energy-dispersive X-ray spectroscopy (EDXS). Fig. 4 reports the results of these analysis: steel (identified as 100 % Fe due to the absence of carbon measurements), chromite (characterized by its intermediate gray color and angular geometry), wüstite (light gray phase), and larnite (dark gray phase). Additionally, brownmillerite was identified as an acicular (needle-like) phase, further indicating its role in the chromium leaching behaviour.

Leaching tests, assessed the release of Cr, V, and Mo from both free

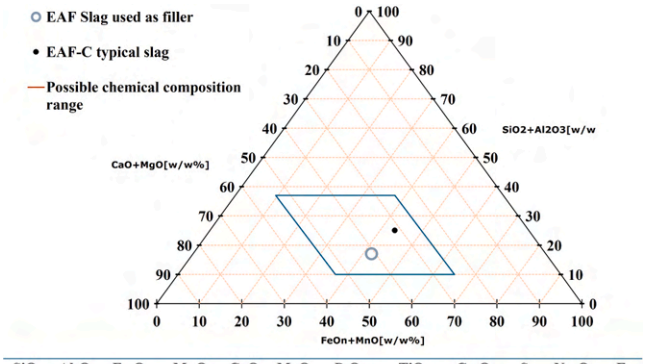

SiO_2	Al_2O_3	Fe_2O_3	MnO	CaO	MgO	P_2O_5	TiO_2	Cr_2O_3	S	Na_2O	F
9.4%	6.4%	33.7%	6.9%	30.1%	5.9%	0.5%	0.4%	6.1%	0.1%	0.4%	0.1%

Fig. 1. Ternary plot of EAF slag chemistry (CaO + MgO / SiO_2 + Al_2O_3 / FeO_n + MnO, wt%) showing the typical compositional range of carbon steel EAF slag according to the REACH Ferrous Slag Consortium. The marker indicates the chemical composition of the EAF slag used in this study, determined by x-ray fluorescence spectroscopy (XRF) analysis %wt [9].

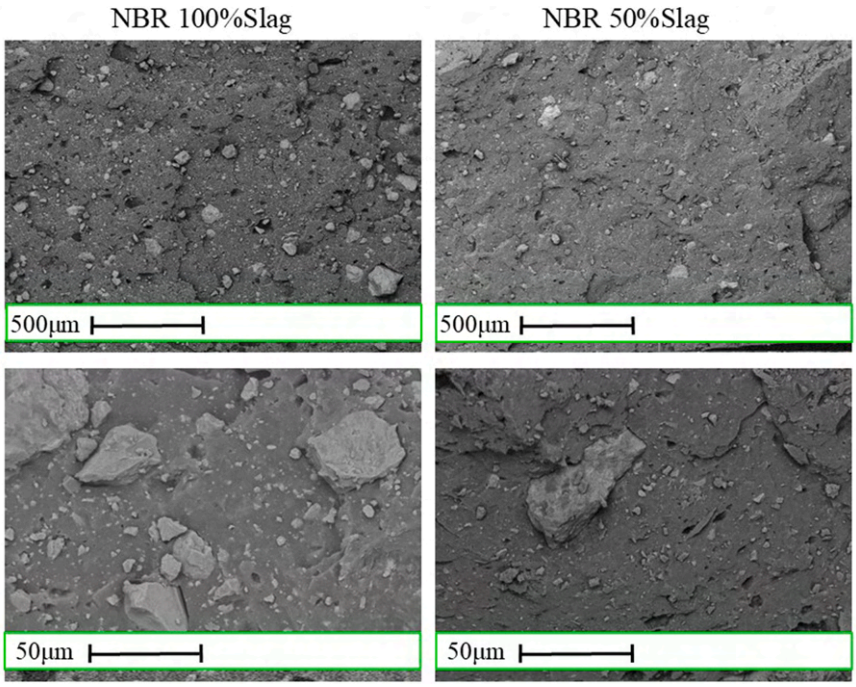

Fig. 2. SEM micrograph of cross sections of EAF slag filled NBR specimens broken in liquid nitrogen.

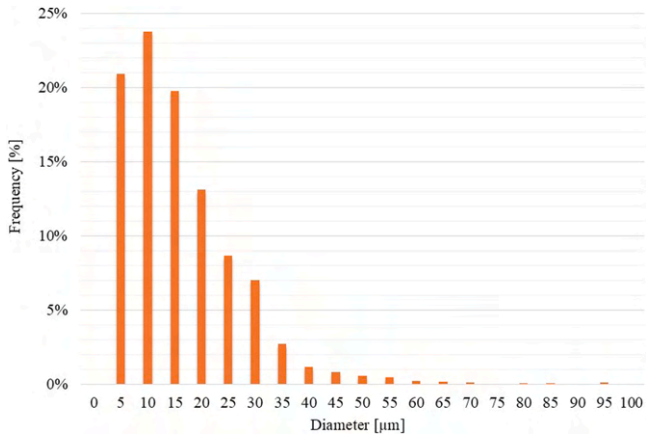

Fig. 3. EAF slag particles granulometric distribution. Data based on [9].

slag and slag embedded in the compound. Fig. 5 shows that free slag leached more Cr and V when in a coarser grain size, likely due to the dissolution of larnite, which increases Ca concentration in the leachate, thereby reducing V leaching. In contrast, the embedding of slag into the NBR significantly reduced the release of these elements, demonstrating the matrix's effective shielding effect. The leachate levels were well within the regulatory limits for both material reuse and disposal as inert material under Italian legislation (Ministerial Decree n. 186, 2006 and Ministerial Decree n. 201, 2005) [20,21].

3.2. Composites characterization

3.2.1. Processability

3.2.1.1. Rheometric properties. The rheometry traces provide detailed information on three key features of elastomer formulations. Firstly, there is the processing behaviour (phase 1). Secondly, there is the dynamics of vulcanisation (phase 2). And thirdly, there are the ultimate physical attributes (phase 3). Each phase provides valuable information about material behaviour throughout the manufacturing process.

Fig. 6 presents a comparative overlay of rheometric curves at 177°C (350 °F), i.e., the standard industrial curing temperature, for the three formulations under investigation. The data reveals that partial substitution of carbon black with EAF slag produces notable effects on compound behaviour. The scorch time (t_{s1}) exhibits a slight extension in slag-containing formulations, indicating a marginally improved processing safety window. Remarkably, the time to 90 % cure (t_{90}) remains virtually unchanged across all formulations, demonstrating that the overall vulcanization rate is preserved despite modifications to the filler composition.

The most pronounced difference between the formulations appears in the maximum torque (M_H) values, which strongly decrease with increasing slag content. This trend suggests a corresponding reduction in polymer-filler interaction and crosslink density, which ultimately influences the mechanical performance of the vulcanizates [9]. Simultaneously, the minimum torque (M_L) shows a slight decrease with increasing slag content, indicating a modest reduction in compound viscosity.

This behaviour can be attributed to two primary factors. First, the surface chemistry difference between the fillers plays a significant role: carbon black establishes strong physicochemical interactions with the elastomer matrix through its high surface activity and functional groups [22], while EAF slag, despite possessing certain reactive surface sites, predominantly functions as a semi-reinforcing filler with less pronounced polymer-filler interactions. Second, the particle size disparity between carbon black (typically 20–50 nm) and EAF slag (up to 100 µm) results in a substantially different specific surface area available for polymer interaction, with carbon black offering orders of magnitude greater interfacial contact area.

The temperature dependence of the vulcanization process for all three formulations across five different temperatures (165°C, 177°C, 185°C, 195°C, and 200°C) is reported in supplementary material as Figure a. As expected from vulcanization theory, increasing temperature produces three consistent effects across all formulations: (i) a reduction in maximum torque (M_H), indicating lower crosslink density at elevated temperatures due to competing degradation reactions; (ii) a decrease in minimum torque (M_L), reflecting reduced compound viscosity at higher

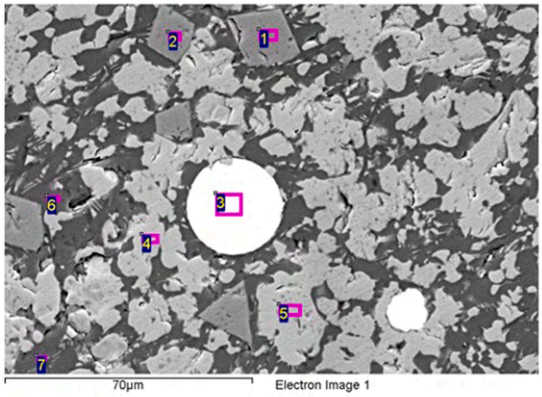

Spectrum	O	Mg	Al	Si	Ca	Cr	Mn	Fe	Phase
1	27	7	3		1	44	4	14	Chromite
2	27	8	3		1	44	4	13	Chromite
3								100	Steel
4	18	5			2	3	10	62	Mg Wuestite
5	21	5	1		2	3	10	58	Mg Wuestite
6	35			16	39		2	9	Lamite
7	36			17	45			2	Lamite

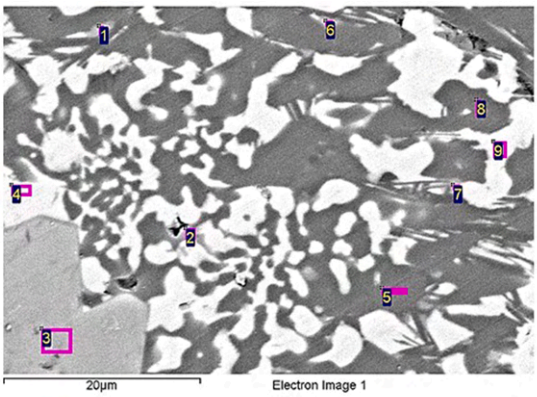

Spectrum	O	Mg	Al	Si	Ca	Ti	V	Cr	Mn	Fe	
1	35		6	8	35	7	1	1		7	Brownmillerite
2	31			12	29			1	3	22	Brownmillerite
3	26	7	3		1			47	4	13	Chromite
4	22	4		2	6			2	8	55	MgWuestite
5	35		1	17	45					3	Lamite
6	32		12	5	27	2			3	20	Brownmillerite
7	32		6	9	36	7	1	1		10	Brownmillerite
8	36			15	44				1	4	Lamite
9	22	3	2	2	5			1	9	55	MgWuestite

Fig. 4. A scanning electron microscope (SEM) back-scattered electron (BSE) image of the microstructure of a metallographically polished EAF slag sample.

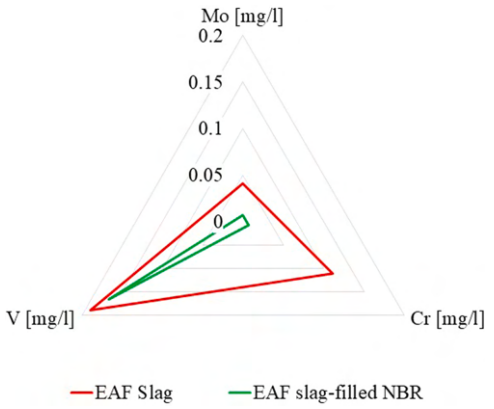

Fig. 5. Maximum concentrations of Cr, V, and Mo detected in the eluate from leaching tests conducted on free slag (according to CEN EN 12457–2) and on slag incorporated into the compound.

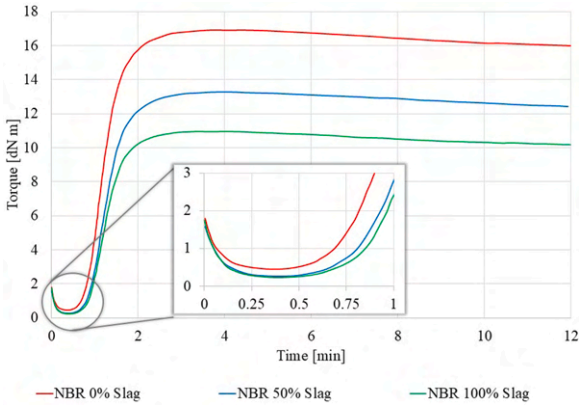

Fig. 6. Rheometric curve of NBR 0 % slag, NBR 50 % slag and NBR 100 % slag, 177°C.

temperatures; (iii) an accelerated vulcanization kinetics, manifested as shorter scorch times (t_{s1}) and cure times (t_{90}) [23].

These temperature-dependent behaviours follow established principles of rubber vulcanization, with the accelerated reaction rates at higher temperatures enabling faster processing but potentially compromising ultimate mechanical properties. Most notably, the parallel shifts in rheometric profiles across temperatures for all formulations suggest that the thermal sensitivity of the vulcanization reaction remains relatively consistent regardless of filler composition.

To quantitatively assess the vulcanization kinetics, the rheometric data was normalized according to Eq. 1 to determine the degree of crosslinking (α) with respect to time. The normalized curves for all three formulations across the full temperature range are reported in supplementary material as Figure b. The remarkable overlap of these curves confirms that the vulcanization reaction rate is minimally affected by the substitution of carbon black with EAF slag. This consistency in cure rate across formulations is particularly advantageous from a manufacturing perspective, as it eliminates the need for process adjustments when incorporating slag as a partial replacement for carbon black.

Further analysis of the vulcanization kinetics was conducted using the Arrhenius approach. Assuming first-order reaction kinetics, the apparent cure rate constant (k) was determined at each temperature by linear regression analysis [24]. Fig. 7 presents the Arrhenius plots (ln k versus 1000/T) for all three formulations, which exhibit nearly identical slopes. The activation energies (E_a) derived from the Arrhenius plot slopes reveal remarkably consistent values across all three formulations: 98 kJ/mol for the standard carbon black-filled NBR (0 % slag), 92 kJ/mol for the composite formulation (50 % slag), and 99 kJ/mol for the fully slag-substituted compound (100 % slag). These minor variations fall within the experimental uncertainty range, indicating no significant difference in the temperature dependence of the vulcanization reaction regardless of filler composition.

This consistency in activation energy values provides compelling evidence that the fundamental crosslinking mechanism remains unaltered when carbon black is partially or completely replaced by EAF slag. The activation energy represents the required energy threshold for the vulcanization reaction to proceed, and its invariance across formulations suggests that the sulphur-accelerator chemistry that governs network formation operates independently of the filler type present in the

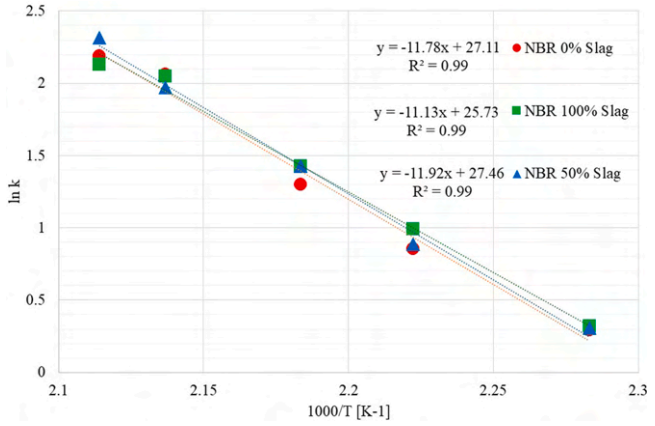

Fig. 7. ln k versus (1/T), from Arrhenius equation of NBR 0 % slag, NBR 50 % slag and NBR 100 % slag, at 165°C, 177°C, 185°C, 195°C, 200°C.

compound.

Viscosity was measured by means of an RPA over a range of oscillation frequencies to evaluate the effect of slag on flow behavior at high shear rates, taking into account the Cox–Merz empirical relationship. It has been established [25] that, for many polymer systems, the steady-shear viscosity η evaluated as function of shear rate $\dot{\gamma}$ corresponds to the complex viscosity η* reported versus angular frequency ω.

Under injection-molding conditions, high shear forces disrupt the filler–filler network, leading to a reduction in viscosity—an effect not observed in conventional RPA protocols. To reproduce this network breakdown within the RPA, a pre-shear treatment was applied during the 4 min temperature ramp prior to testing, following the method of Fasching [26]. For an NBR compound, it was shown that a 3° strain amplitude at 5 Hz is sufficient to dismantle the filler network without damaging the polymer chains. By comparing viscosity curves obtained with and without this pre-shearing step, the integrity of the filler network can be inferred: a lower viscosity indicates network disruption.

Fig. 10 presents the complex viscosity η* (ω) for CB-filled NBR, NBR filled entirely with EAF slag, and a NBR (50 % slag). Solid lines denote measurements without pre-shear, while dashed lines represent pre-sheared samples. NBR (0 % slag) exhibits a slightly higher complex viscosity compared to the slag-filled formulations, and no substantial difference is observed between the 100 % and 50 % slag/NBR blends, in agreement with the MDR results.

Fig. 9 reports both the absolute reduction in complex viscosity (Δη) and the corresponding percentage decrease for clarity. Although Δη in Pa·s diminishes with increasing frequency, the baseline viscosity η* (without preshearing) rises much more steeply at low frequencies, so that the ratio Δη/η* (and hence the % reduction) remains high or even increases as frequency decreases.

The data reveals an exponential decrease in complex viscosity reduction caused by pre-shearing as angular frequency increases. This behaviour stems from the shortened observation time at higher frequencies, which prevents complete disruption and reconstruction of the filler network, thereby diminishing its overall influence on the system's properties.

This reduction is most pronounced in carbon black-filled NBR and decreases progressively with increasing slag content as replacement. This phenomenon can be attributed to the complex interplay between bound rubber and filler-matrix interactions. The polymer layer physically or chemically adsorbed onto the filler surface exhibits higher rigidity compared to free polymer and acts as an interfacial transition between the filler phase and polymeric matrix. In systems containing reinforcing fillers such as carbon black, bound rubber significantly enhances both rigidity and complex viscosity by strengthening filler-matrix interactions.

During pre-shearing, high shear forces disrupt the physical and chemical interactions between filler and matrix, compromising bound rubber integrity. While this disruption is not complete, it reduces the bound rubber's structural contribution, resulting in decreased complex viscosity post-pre-shearing. The magnitude of this effect varies with filler type and content. Systems with less reinforcing fillers exhibit weaker filler-filler networks and consequently less significant bound rubber contributions, leading to less pronounced decreases in complex viscosity. Conversely, highly reinforcing systems demonstrate synergistic effects between the filler-filler network and bound rubber, where partial destruction of both during pre-shearing amplifies the reduction in viscoelastic properties.

The frequency dependence of this phenomenon is particularly noteworthy. At lower angular frequencies, longer observation times enable the system to manifest collective behaviour of filler, matrix, and their interactions, making bound rubber's contribution more significant. However, at higher frequencies, where local and dynamic responses of

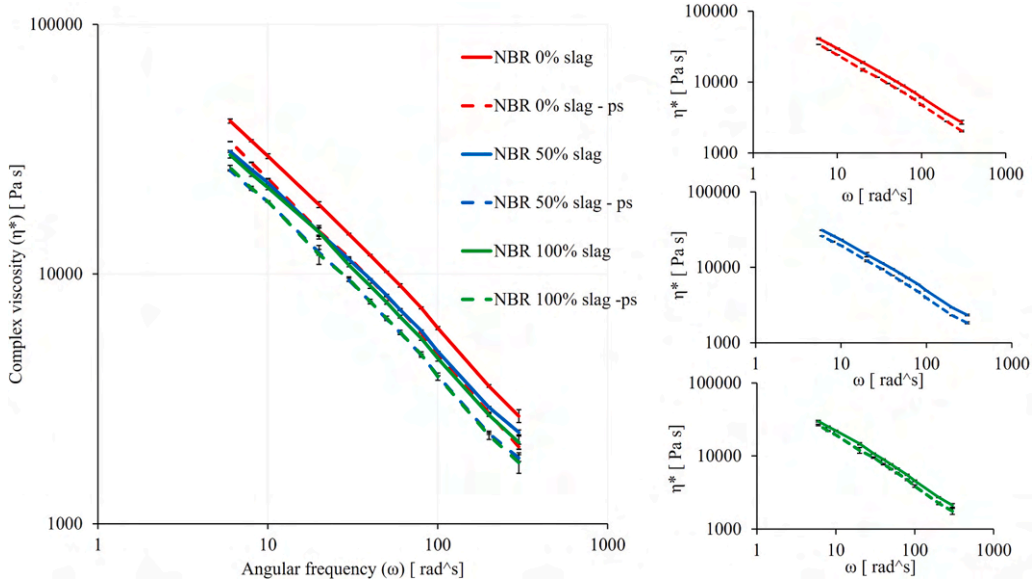

Fig. 8. Variation of complex viscosity with angular frequency of NBR 0 % slag, NBR 50 % slag and NBR 100 % slag. The solid lines indicate the complex viscosity of the three formulations without pre-shearing, while the dotted lines correspond to measurements performed after applying pre-shearing (ps).

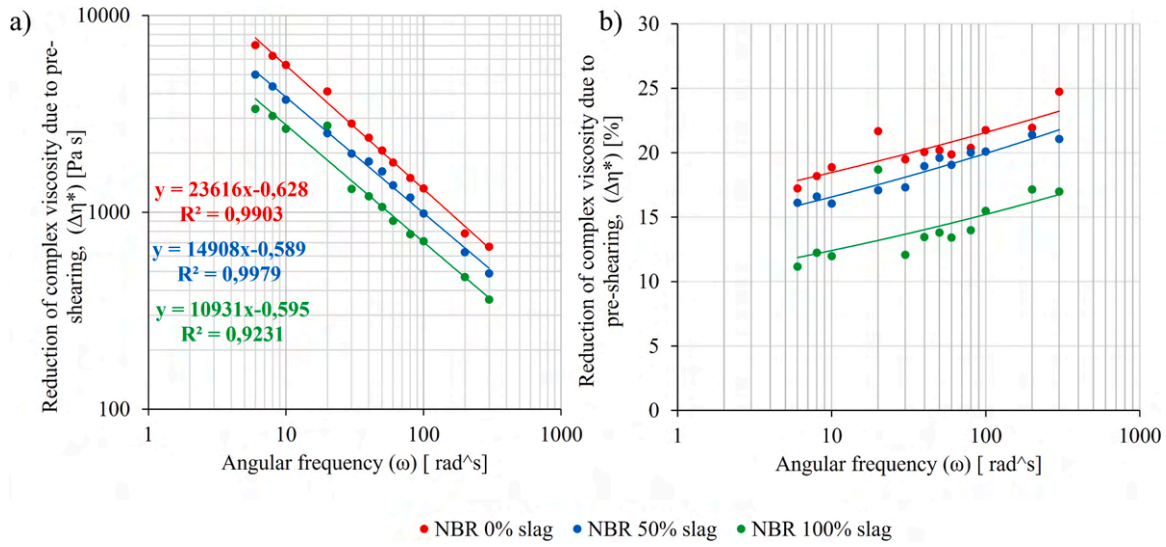

Fig. 9. Reduction of complex viscosity due to pre-shearing (Δη*)in absolute terms [Pa·s] (a) and in percentage [%] (b) as functions of angular frequency (ω) of NBR 0 % slag, NBR 50 % slag and NBR 100 % slag.

free polymer chains dominate, bound rubber's influence diminishes, explaining the attenuation of complex viscosity reduction with increasing frequency.

he results show that the NBR compound without slag (0 %) demonstrates the highest degree of reinforcement, with the 50 % and 100 % slag-filled formulations displaying progressively lower reinforcement levels. Nevertheless, at higher frequencies (47.75 Hz or ω=300 rad/s) the viscosity values of all three compounds converge, showing nearly identical reductions.

3.2.1.2. Industrial processability via injection moulding. The processability of NBR compounds filled with EAF slag was evaluated through industrial injection moulding. Fig. 10 presents images of the rubber parts inside the mould before demoulding under standard processing conditions, alongside those produced using optimized moulding parameters. Despite laboratory tests not revealing significant differences in cure kinetics or viscosity, injection moulding trials exposed certain critical issues. This discrepancy is attributed to the high deformation rates typical of injection moulding, which are significantly greater than those in standard rheological testing. Under such conditions, the compound does not behave as a homogeneous material; instead, the two-phase nature—comprising a soft elastomeric matrix and a hard particulate filler—becomes more pronounced. Specifically, the weak interfacial adhesion between the matrix and the slag filler appears to be disrupted, reducing the ability of the phases to deform cooperatively and undermining the compound's flow behavior during mould filling. NBR 50 % slag showed greater difficulty in achieving balanced filling of the mould cavities, while NBR 100 % slag faced challenges in reaching complete cavity fill, leading to the production of several faulty components. For these reasons, as anticipated, the processing conditions cannot yet be

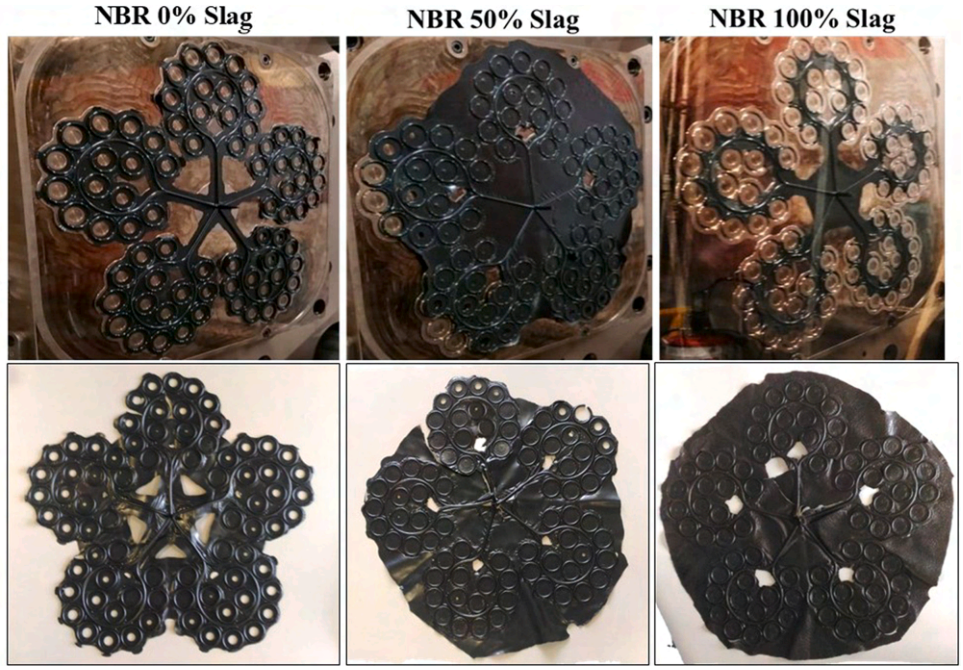

Fig. 10. Images of injection moulded rubber parts produced by injection moulding with NBR 0 % slag, NBR 50 % slag and NBR 100 % slag. Top: in-mould parts under optimal conditions for NBR 0 % slag (commercial compound). Bottom: parts with optimized process parameters for each. Process parameters in Table 2.

considered optimized for full-scale production. Nevertheless, parts were successfully obtained and are shown in Fig. 10.

The industrial processability study was conducted under different moulding conditions for each compound, selecting parameters that optimize moulding performance accordingly. In particular, as the slag content increased, higher injection speed and pressure were required. The most critical issue identified was the difficulty in filling the mould when slag was used as a filler, which is likely due to the coarse particle size of the slag. Specifically, since rheological studies did not reveal significant differences between the compounds, this difficulty can be attributed to the inability of coarse slag particles to flow into the smaller mould cavities.

In the case of the NBR 50 % slag compound, a partial and unbalanced filling was achieved, whereas for the NBR 100 % slag compound, cavity filling was barely initiated, and the flow was interrupted at the cavity gate. This phenomenon is likely caused by the mechanical blockage of the gates (approximately 0.05 mm thick) by slag particles (up to 0.1 mm), leading to a clogging effect that obstructed the passage of the compound.

In order to gain more information about the injection moulding processability, this work adopted a methodology for online process monitoring developed by some of the authors [27].

The procedure is based firstly on the measurement of the shear heating temperature, T_{SH}, i.e. the rubber surface temperature at the nozzle outlet of the injection moulding machine extruder, which is measured by an infrared thermal camera. In fact, during injection moulding, shear heating phenomena can increase the temperature of rubber compounds in an unpredictable way. Shear heating is the temperature rise caused by internal friction within the rubber, while it is flowing. The temperature rise has influence both on viscosity and on curing kinetics, thus affects product quality. As laboratory tests, such as MDR tests, cannot replicate exactly the shear heating phenomenon occurring in a moulding machine, the direct measurement with a thermal camera of rubber surface temperature, where the rubber leaves the extruder barrel, allows monitoring this effect and provides a better control over the process.

T_{SH} values measured from thermal images and averaged over a short extrudate section close to the nozzle are (see also Table 3 below): 146°C for NBR 0 % slag, 156°C for NBR 50 % slag and 145°C for NBR 100 % slag. T_{SH} of NBR 50 % slag is about 10°C higher with respect to NBR 0 % slag. This shear heating temperature increase wasn't attributable to EAF slag addition, but it was reasonably attributable to the increased injection pressure and injection speed, set to improve the injection stage. NBR 100 % slag and NBR 0 % slag have very similar T_{SH}. Therefore, a high percentage of EAF slag didn't affect the temperature of shear heating.

Furthermore, using T_{SH} values it is possible to measure the corresponding shear heating parameter, ηSH [27], a technological parameter related to rubber viscosity, which considers not only physical material properties (density and specific heat capacity), but also process conditions (screw L/D ratio). The shear heating parameter is calculated according to the Eq. 7:

$$\eta_{SH} = (T_{SH} - \mathrm{RT})\frac{\rho c_p}{4\nu} \bullet \frac{D}{L} \tag{7}$$

Table 3
Experimental results for the shear heating analysis.

		NBR 0 % Slag	NBR 50 % Slag	NBR 100 % Slag
Shear heating temperature, T_{SH}	[°C]	146	156	145
Density, ρ	[kg/m^3]	1206	1433	1654
Specific heat capacity @T_{SH}, c_p	[J/(kg·K)]	1883	1601	1641
ηSH	[Pa·s]	$4.47{\cdot}10^5$	$4.88{\cdot}10^5$	$5.30{\cdot}10^5$

where ηSH [Pa·s] is the shear heating parameter, RT [K] is room temperature (here equal to 20°C), ρ [kg/m^3] is the rubber density, c_p [J/kg·K] is the specific heat capacity at T_{SH}, ν [s^{-1}] is a flow rate parameter, here set to 10 s^{-1}, as this is a shear rate order of magnitude common in extrusion processes, and D/L is the screw diameter over length ratio. The calculated ηSH value combines both rubber composition and operating condition effects, giving more information about the actual thermal history of the rubber injection stage and process safety than M_L values, which are measured via laboratory tests under standard conditions.

Table 3 shows processing-related results of the formulated compounds, and the ηSH results calculated with Eq. 7.

The shear heating parameter, ηSH, resulted equal to $4.47{\cdot}10^5$ Pa·s for NBR 0 % slag, $4.88{\cdot}10^5$ Pa·s for NBR 50 % slag and $5.30{\cdot}10^5$ Pa·s for NBR 100 % slag. Therefore, the use of EAF slag in NBR rubber compounds has increased ηSH. Nevertheless, this ηSH increase was not directly related to shear heating temperature (not significantly increased), but it was mainly due to the increase of rubber density with the introduction of EAF slag.

Despite the introduction of slag into NBR reduced the minimum torque, M_L, by MDR (see Fig. 6 and), the processing characterization highlighted some critical moulding issues. Therefore, the increase of the parameter of shear heating has confirmed the difficult processability of the two slag filled rubber compounds, and also in this experiment it proved to be much more reliable than M_L in providing indication about processability.

Pseudoplastic materials exhibit strong shear-rate dependency in their viscosity behavior, making it critical to correlate laboratory rheometric measurements with actual processing conditions where significantly higher shear rates are encountered. This correlation is essential for accurate process design and optimization.

The selected process, i.e. injection molding, presents particular issues due to its demanding flowability requirements and the restrictive geometry of mold channels. Analysis indicates that the primary obstacle to successful cavity filling stems from the relatively large particle size of the incorporated slag.

The industrial mold configuration, featuring 174 cavities fed through a single central gate, imposes high deformation rates during both injection and filling phases. Under these severe flow conditions, the elastomeric polymer matrix (the "soft" phase) experiences significant viscosity reduction and flows readily. However, the slag particles (the "hard" phase), with their substantially larger mean diameter compared to conventional carbon black, cannot effectively track the advancing flow front. This disparity leads to phase separation and heterogeneous flow behavior, with the severity increasing proportionally to slag loading.

While the current process and mold configuration were intentionally selected to highlight potential processing limitations, several mitigation strategies can address these challenges through both mold design modifications and alternative processing approaches.

Mold design modifications offer the most direct path to improving processability within the existing injection molding framework. Reducing the cavity count from 174 to a more manageable number such as 4 cavities significantly decreases overall flow resistance and allows for more controlled filling dynamics. Additionally, expanding the cross-sectional areas of the runner system reduces pressure losses throughout the flow network, enabling more uniform material distribution. Gate geometry optimization represents another critical modification, where careful design can minimize local shear rates and substantially reduce the flow path lengths required to fill each individual cavity.

Alternative processing technologies provide viable pathways when conventional injection molding modifications prove insufficient. Injection-compression molding represents a particularly promising hybrid approach that combines the precision of injection molding with the gentler processing conditions of compression molding. This method involves partial cavity filling through conventional injection, followed by compression to achieve the final part geometry. By eliminating the

Table 4
Tensile, compression test and permanent set results of NBR 0 % slag, NBR 50 % slag and NBR 100 % slag [9].

Test	Compound	E(100 % strain) [MPa]			Stress at break [MPa]			Strain at break [%]		
Tensile	**NBR 100 % Slag**	1.19	±	0.04	5.41	±	0.50	344	±	19
	NBR 50 % Slag	1.53	±	0.04	9.38	±	0.20	393	±	9
	NBR 0 % Slag	2.41	±	0.04	13.56	±	0.88	378	±	16
		E_c [MPa]					**Stress at 45 % strain [MPa]**			
Compression	**NBR 100 % Slag**	4.58	±	0.11			3.84	±	0.89	
	NBR 50 % Slag	5.50	±	0.14			4.16	±	0.03	
	NBR 0 % Slag	8.72	±	0.19			5.42	±	0.25	
		Compression set [%]								
Permanent set	**NBR 100 % Slag**	13.7	±	0.2						
	NBR 50 % Slag	14.8	±	0.4						
	NBR 0 % Slag	13.2	±	0.6						

need for conventional gates and their associated high-shear zones, this technique significantly reduces the compound's exposure to damaging shear stresses while maintaining excellent dimensional precision and surface quality.

Compression molding offers the most straightforward alternative for applications where high-shear processing proves problematic. Laboratory-scale validation studies have confirmed that conventional compression molding remains fully compatible with NBR-slag compounds across a range of formulations and processing conditions. This approach provides a reliable, low-shear alternative that preserves the integrity of the slag-polymer system while delivering consistent part quality and mechanical properties.

The processing challenges observed with NBR-slag compounds are primarily attributable to the large particle size of EAF slag (up to 100 μm) relative to narrow mold dimensions (gates ≈50 μm), which causes mechanical obstruction and phase separation under high-shear injection conditions, rather than fundamental chemical incompatibilities or intrinsic rheological deficiencies of the compound. Through appropriate process selection and mold design optimization, these compounds can be successfully manufactured while maintaining their desired properties and performance characteristics.

3.2.2. *Physicochemical characterization*

3.2.2.1. Thermal conductivity. In Fig. 11, the thermal conductivity of NBR compounds filled with carbon black, 100 % EAF slag, and 50 % EAF slag is illustrated. The results demonstrate that the incorporation of slag does not exert a substantial influence on the thermal conductivity of the material, thereby indicating that the heat transfer properties remain unaltered. Consequently, the vulcanization kinetics, which is influenced by the thermal conductivity, is not adversely impacted by the slag content. This outcome agrees with the rheometry measurements.

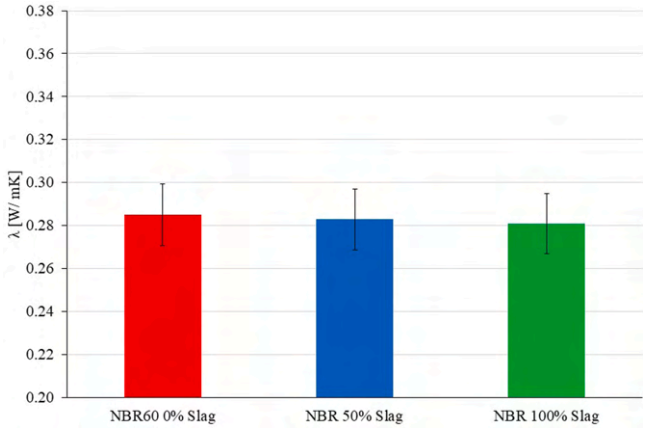

Fig. 11. Thermal conductivity (λ) of NBR 0 % slag, NBR 50 % slag and NBR 100 % slag determined according to ASTM E1530 [18].

3.2.2.2. ATR/FTIR. Attenuated Total Reflectance–Fourier Transform Infrared (ATR-FTIR) spectroscopy was employed to elucidate the chemical structure of three NBR compounds differing only in filler: NBR 0 % slag, NBR 50 % slag and NBR 100 % slag (Fig. 12). All spectra exhibit an intense absorption at ~2237 cm^{-1} , attributable to the C≡N stretching vibration of the nitrile group, indicating that neither partial nor total substitution of carbon black with slag alters this defining functional group. In the aliphatic region, the asymmetric and symmetric CH_2 stretching bands at 2917–2919 cm^{-1} and 2848–2849 cm^{-1} , respectively, remain coincident in position and intensity across all three formulations, confirming preservation of the hydrocarbon backbone [28]. Moreover, the fingerprint region (1500–600 cm^{-1}) shows overlapping C–H bending, C–C stretching and CH_2 deformation bands with no new features or shifts, further demonstrating that the base polymer chemistry is unmodified by the introduction of EAF slag. These results highlight that the primary molecular architecture of NBR is maintained regardless of filler type or loading, and that any changes in macroscopic properties must therefore arise from altered polymer–filler interactions rather than from chemical modifications of the rubber matrix.

3.2.2.3. Thermogravimetric analysis (TGA). TGA is a widely employed technique for evaluating decomposition behaviour and the thermal stability of materials under controlled heating conditions. By continuously measuring the mass loss of a sample as a function of temperature or time, TGA provides critical insights into degradation mechanisms, thermal resistance, and the composition of volatile and non-volatile fractions. This technique is particularly valuable in the characterization of polymers, composites, and flame-retardant materials, as it allows for the identification of key degradation stages, onset decomposition temperatures, and char residue formation. The thermal stability of a material, as determined by TGA, is essential for evaluating its suitability for high-temperature applications, as well as for optimizing formulations to enhance fire resistance and longevity.

Fig. 13 displays the temperature-dependent weight loss profile,

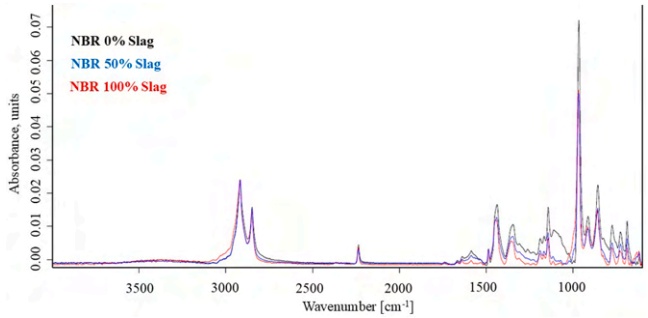

Fig. 12. ATR-FTIR scan of NBR 0 % slag, NBR 50 % slag and NBR 100 % slag.

highlighting four distinct decomposition stages corresponding to the main components of the compound. The initial weight loss, occurring between approximately 200–400 °C, is attributed to the evaporation of volatile substances. A second, more significant drop between 400–550 °C is linked to the degradation of the polymer matrix. The subsequent decline from 550 to 600 °C corresponds to the combustion of carbon black. Beyond this point, the weight stabilizes, indicating the presence of non-combustible residues—primarily ash and inorganic fillers.

It was determined that pure NBR contains roughly 3 % residual ash, which was subtracted from the total inorganic residue measured in slag-filled samples to accurately calculate the slag loading. The carbon black content was quantified as the mass loss occurring during the oxidative step, corresponding to the combustion of carbonaceous species after polymer degradation under nitrogen. The analysis confirmed that both the carbon black and slag contents align with their intended formulation values. The TGA analysis indicates that the thermal stability of the NBR composites is significantly influenced by the filler composition. Slag-filled formulations exhibit a progressively lower mass loss up to 400°C, proportionally to the slag content, compared to NBR with 0 % slag, suggesting that the presence of EAF slag enhances thermal resistance. In particular NBR 100 % slag shows a weight reduction of 12 %, NBR 50 % slag 14 % and NBR 0 % slag 16 % at 400°C.

This behaviour can be attributed to the intrinsic thermal stability of the primary slag oxides belonging to the $CaO–SiO_2–Fe_2O_3$ system, whose melting temperatures are significantly higher that the decomposition temperature range of the NBR matrix. During thermal degradation of the rubber matrix (≈400–550°C), these oxides remain chemically inert and structurally stable.

In addition, the dispersed slag particles exert a physical barrier effect by increasing the tortuosity of diffusion pathways for oxygen diffusion into the bulk material and restricts the escape of volatile degradation products, thereby slowing down the overall decomposition kinetics. The presence of a thermally stable inorganic phase also increases the thermal inertia of the composite, contributing to a moderation of local thermal gradients during the early stages of degradation (200–400°C). In contrast, the higher carbon black content in NBR 0 % slag may promote more pronounced thermal degradation due to its different interaction mechanism with the polymer matrix. These findings are consistent with literature reports on the flame-retardant behaviour of steel slag in polymer systems [29]

The morphological and surface differences between carbon black and EAF slag further contribute to the observed thermal behaviour of the NBR conposites. Carbon black consists of nanoscale particles, which generate an extensive polymer–filler interfacial area and can influence the thermal degradation behaviour of elastomers.

In contrast, the EAF slag particles used in this work are micrometric in size, resulting in a markedly lower polymer–filler interfacial area. Consequently, surface-mediated effects on polymer degradation are expected to be limited. Instead, the dispersed slag particles primarily act through a physical barrier mechanism, increasing the diffusion path length for volatile degradation products and thereby retarding their release during thermal decomposition.

This barrier-dominated behaviour, combined with the intrinsic thermal stability of the slag oxides, is consistent with the progressively reduced mass loss observed with increasing slag content in the TGA results.

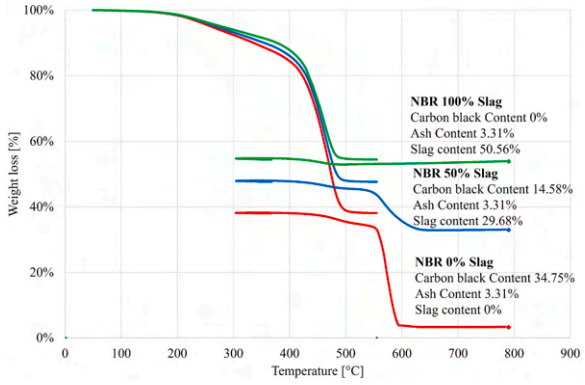

Fig. 13. Thermogravimetric scan of NBR compounds containing 50 % and 100 % EAF slag measured at 10 °C/min under nitrogen atmosphere from 25 to 550 °C and under oxygen atmosphere from 550 to 800 °C. The final residue values have been corrected by subtracting the intrinsic ash content of neat NBR (≈3 wt%), so that the reported residue corresponds to the contribution of the EAF slag filler.

3.2.2.4. Differential scanning calorimetry (DSC). DSC was performed to determine the glass transition temperature (T_g) of the NBR composites and to assess the potential influence of different fillers on the polymer's thermal behaviour. The DSC thermograms are reported in supplementary material as Figure c and reveal that the T_g remains constant at approximately −25.5°C across all formulations, regardless of the slag or carbon black content. This indicates that the incorporation of EAF slag or carbon black does not significantly alter the mobility of the polymer chains within the elastomeric matrix. The lack of variation in T_g suggests that the fillers primarily act as passive reinforcing agents without disrupting the segmental dynamics of the NBR phase, in agreement with ATR-FTIR findings.

3.2.3. Mechanical characterization

An extensive mechanical characterization of NBR composites reinforced with carbon black and EAF slag has been reported in [9]. The tensile test results indicate a progressive reduction in both stiffness and tensile strength with increasing slag content. The carbon black-filled NBR (0 % slag) exhibited the highest tensile modulus at 100 % strain (2.41 MPa) and maximum tensile strength (13.56 MPa), with an average strain at break of 378 %. The composite with 50 % slag showed intermediate properties, with a tensile modulus of 1.53 MPa, a tensile strength of 9.38 MPa, and a slightly higher average strain at break of 393 %, suggesting a slight increase in extensibility. In contrast, the composite with 100 % slag demonstrated the lowest tensile performance, with a modulus of 1.19 MPa, a tensile strength of 5.41 MPa, and an elongation at break of 344 %.

Similarly, the compression test results reveal that the 0 % slag composite possessed the highest compressive modulus (E_c) of 8.72 MPa and a stress of 5.42 MPa at 45 % strain. The 50 % slag composite exhibited reduced compressive properties, with E_c of 5.50 MPa and a stress of 4.16 MPa at 45 % strain, while the 100 % slag composite showed the lowest values (E_c of 4.58 MPa and stress of 3.84 MPa at 45 % strain).

The permanent set (compression set) results remain statistically indistinguishable across all three compounds. Each formulation exhibits low residual deformation (mean ≈13–15 %) with tight variability (standard deviations ≤0.6 %), indicating consistent elastic recovery. The 50 % slag blend demonstrates only a marginally elevated mean and variability in comparison to the others, likely indicative of slightly weaker filler–rubber interactions. However, complete substitution with slag restores both the average and spread to levels that are essentially identical to the carbon-black reference.

Overall, these results suggest that partial replacement of carbon black with slag provides a balanced compromise between stiffness, strength, and strain at break, whereas complete substitution significantly reduces the mechanical performance.

3.2.3.1. Tear strength. The tear strength data clearly reflect the influence of filler geometry on crack propagation resistance. The reference NBR compound (0 % slag) displayed the highest tear strength at 41.76 N/mm (± 2.87), whereas the intermediate formulation containing

50 % EAF slag exhibited a substantially reduced value of 21.61 N/mm (± 0.79). Complete substitution of carbon black with slag (100 % slag) yielded the lowest tear strength, 9.13 N/mm (± 0.14). This progressive decline in tear resistance was anticipated given the angular and irregular morphology of the EAF slag particles, which act as stress concentrators and produce a pronounced "notch effect" at the filler–polymer interface. Such sharp-edged inclusions facilitate crack initiation and growth under applied load, thereby compromising the material's intrinsic resistance to tearing.

3.2.3.2. Tribological behaviour. Fig. 14 the coefficient of friction (COF) and specific wear rate (Ws) are reported for NBR compounds containing carbon black, 50 % EAF slag, and 100 % EAF slag, tested under both single-direction and reciprocating wear conditions.

The data reveal that increasing the slag content results in a progressive reduction of the COF. However, this improvement in frictional behavior comes at the expense of wear resistance, as evidenced by the higher specific wear rates observed in both testing modes with increasing slag content.

SEM investigation of wear-induced surface degradation (Fig. 15) highlights the incidence of distinct damage mechanisms among the three materials. In the case of NBR without slag, the predominant wear mechanism is stick-slip, particularly evident in the single-way test configuration, where the wear track reveals a characteristic accumulation zone of displaced material, commonly referred to as Schallamach waves [30]. Conversely, for NBR containing 50 % and 100 % slag, the primary wear mechanism is abrasion, driven by the action of slag particles as a third body. However, notable differences emerge between these two compositions. In the NBR 50 % slag compound, the simultaneous presence of carbon black and slag results in the formation of a relatively flat baseline surface, characterized by cavities left by dislodged coarse slag particles and asperities corresponding to partially embedded slag particles within the elastomeric matrix. In contrast, in the NBR 100 % slag compound, this baseline surface is absent, and the wear process is dominated by severe abrasive mechanisms. In this case, slag particles, once detached from the matrix, act as highly angular third-body abrasives with a hardness significantly greater than that of the elastomeric phase, leading to substantial matrix degradation.

The analysis suggests that the NBR 50 % slag composition represents the most favorable condition, as the presence of slag particles effectively reduces the coefficient of friction by decreasing the adhesive interaction at the contact interface. While the specific wear rate shows a slight increase, this effect is primarily attributed to the loss of slag particles, which possess a significantly higher density compared to the rubber matrix.

It should be noted that the specific wear rate was calculated using the measured mass loss. Given that slag exhibits a density approximately four times greater than that of rubber, the detachment of even a small fraction of slag particles corresponds to the removal of a significantly larger volume of the rubber matrix. This aspect should be carefully considered when interpreting wear data, as it provides a more comprehensive understanding of the material loss mechanisms in slag-filled elastomeric composites.

3.3. Comparative overview

Table 5 provides a comprehensive comparison of the three formulations investigated in this study, highlighting their relative performance across key application-relevant categories. The data synthesizes results from processability assessments, mechanical testing, thermal characterization, and tribological evaluation.

Fig. 16 presents a qualitative radar chart offering a rapid visual comparison of the normalized performance metrics for each formulation. Each axis represents a different property category, with values normalized to the NBR 0 % slag formulation baseline (set to 100 %). This visualization facilitates the immediate identification of trade-offs between sustainability objectives and functional performance.

The selection among these formulations should be guided by specific application requirements, with particular consideration of manufacturing process constraints and the acceptable trade-offs between mechanical performance and environmental sustainability.

4. Conclusion

This study evaluated the industrial feasibility of incorporating EAF slag as a sustainable alternative to carbon black in NBR compounds, focusing on injection moulding applications for sealing components. The research extends previous work on mechanical properties to address industrial processability and application-specific performance, providing critical insights into the practical implementation of this sustainable material substitution.

4.1. Advantages

- Consistent vulcanization process: the incorporation of EAF slag maintains similar activation energies (98 kJ/mol for 0 % slag, 92 kJ/mol for 50 % slag, and 99 kJ/mol for 100 % slag) and crosslinking rates across all formulations, ensuring process reliability.
- Thermal and physicochemical stability: slag substitution preserves thermal conductivity values, glass transition temperature

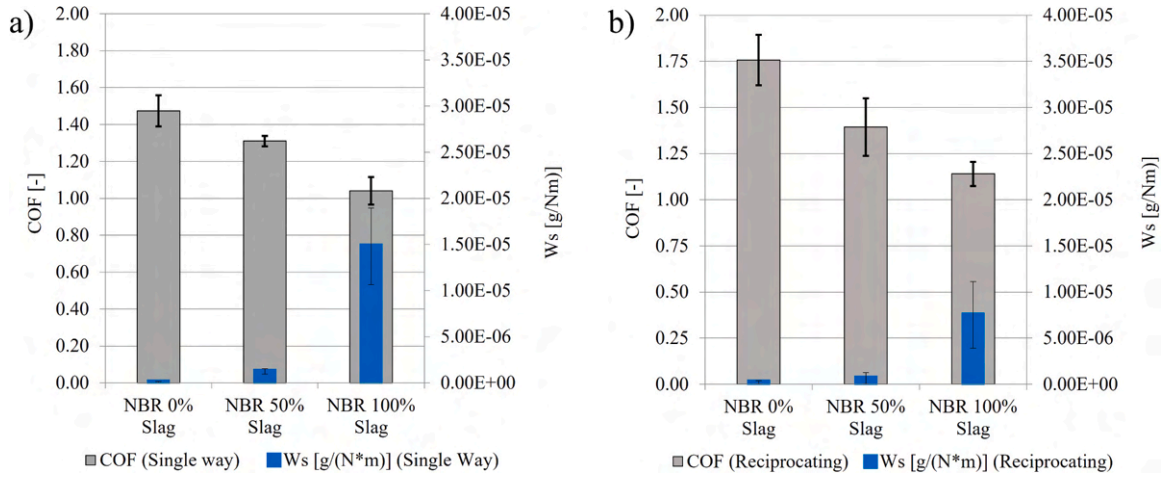

Fig. 14. Specific wear rate (Ws) (a) and Coefficient of friction (COF) (b) measured for NBR compounds containing 0 %, 50 %, and 100 % slag under single-direction and reciprocating wear conditions (5 N load, 200 m sliding distance).

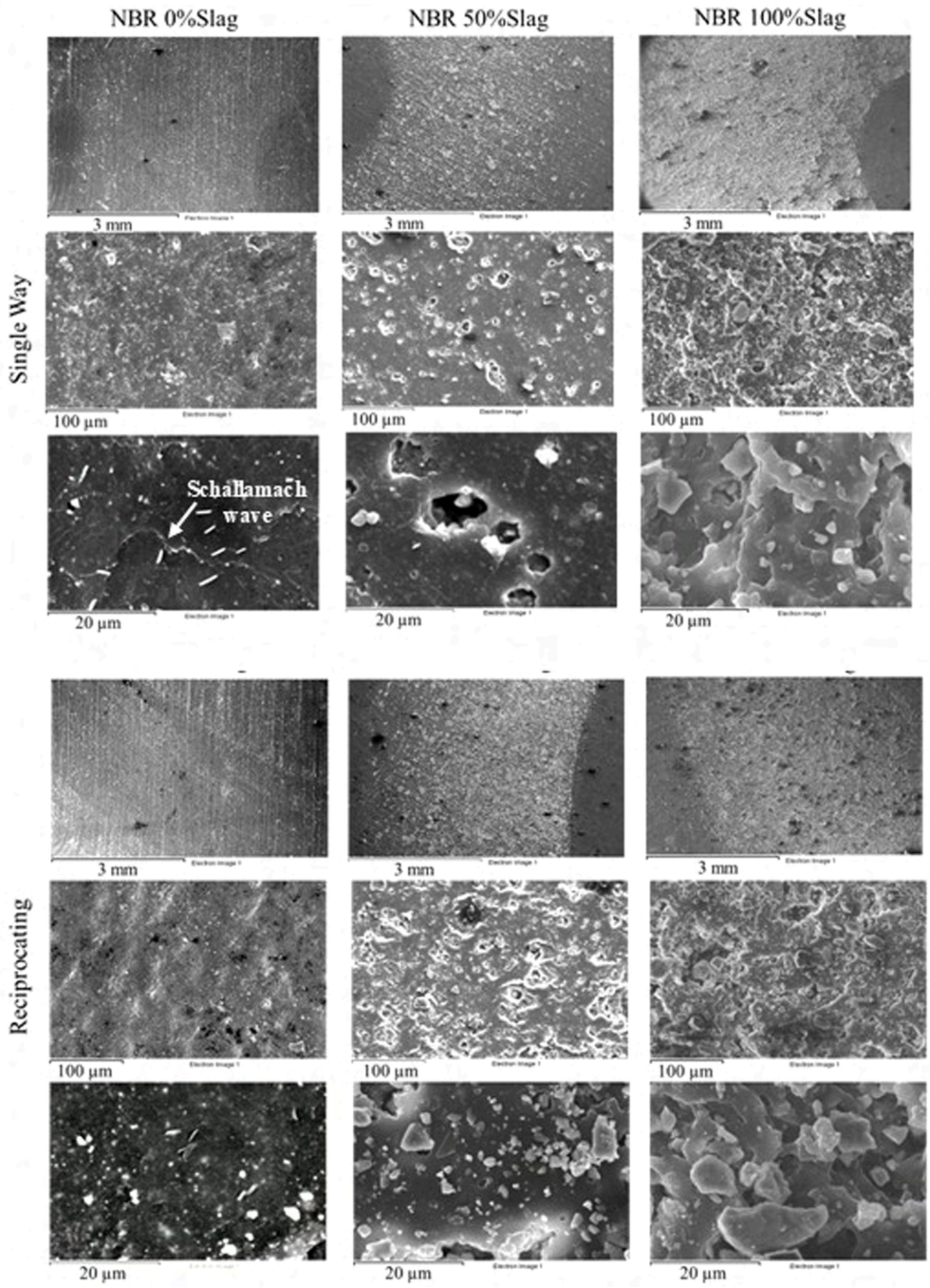

Fig. 15. BSE observations of wear track of NBR 0 % slag, NBR 50 % slag and NBR 100 % slag in single-way and reciprocating wear configuration (5 N, 200 m).

Table 5
Comparative performance summary of NBR formulations.

Property Category	Parameter	NBR 0 % Slag	NBR 50 % Slag	NBR 100 % Slag
Processability	Vulcanization kinetics	Baseline behavior	Unchanged compared to baseline	Unchanged compared to baseline
	Activation energy (kJ/mol)	Baseline value	Comparable to baseline	Comparable to baseline
	Viscosity (ML)	Baseline viscosity	Slightly reduced viscosity	Slightly reduced viscosity
	Injection molding	Excellent processability	Difficult processing due to unbalanced filling	Very difficult processing due to gate blockage
	Compression molding	Excellent processability	Excellent processability	Excellent processability
Mechanical Performance	Tensile strength	Highest tensile strength (reference)	Intermediate tensile strength with moderate reduction compared to carbon black	Lowest tensile strength with marked reduction
	Modulus E100 %	Highest stiffness	Intermediate stiffness	Lowest stiffness
	Tear strength	Highest tear resistance	Significantly reduced tear resistance	Very low tear resistance
	Compression set (%)	Baseline behavior	Comparable to baseline	Comparable to baseline
	Hardness (Shore A)	Highest hardness (reference)	Moderately reduced hardness	Significantly reduced hardness
Thermal Stability	Glass transition temperature (°C)	Baseline glass transition temperature	Unchanged compared to baseline	Unchanged compared to baseline
	Thermal conductivity	Baseline thermal conductivity	Comparable to baseline	Comparable to baseline
	Thermal degradation resistance	Baseline resistance	Slightly enhanced resistance	Enhanced resistance
Tribological Behavior	Coefficient of friction	Baseline coefficient of friction	Reduced coefficient of friction	Strongly reduced coefficient of friction
	Specific wear rate	Baseline wear rate	Moderately increased wear rate	Significantly increased wear rate
	Primary wear mechanism	Stick–slip	Mixed abrasion	Severe abrasion
Environmental Impact	Carbon black content	Full carbon black formulation	Mixed formulation with equal carbon black and slag content	Carbon black fully replaced by slag
	Slag valorization	No slag valorization	Partial slag valorization	Maximum slag valorization
	Petroleum dependence	High dependence on petroleum-based fillers	Medium dependence on petroleum-based fillers	Low dependence on petroleum-based fillers
Overall Assessment	Best suited for	High-performance applications	Balanced sustainability and performance	Maximum environmental benefit
	Main limitation	High environmental impact	Reduced mechanical properties	Poor injection molding performance and low strength

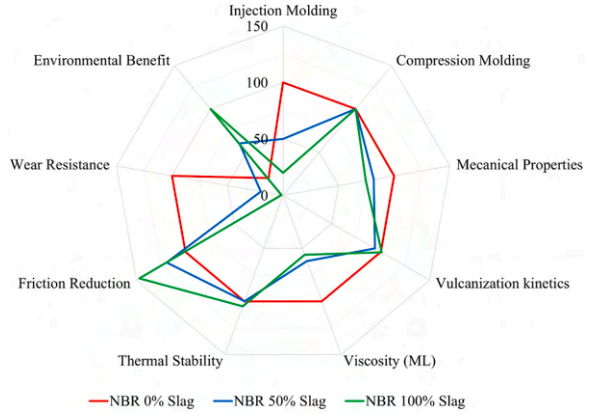

Fig. 16. Normalized radar chart (NBR 0 % slag baseline = 100).

(approximately −25.5°C), and the NBR matrix molecular structure, while TGA results indicate enhanced thermal stability for slag-containing compounds.

- Tribological benefits: decreased friction coefficients with increasing slag content offer advantages for certain sealing applications.
- Environmental impact: the partial replacement of carbon black with EAF slag delivers dual environmental benefits by reducing dependence on petroleum-derived materials while simultaneously valorising an industrial byproduct.

4.2. Limitations

- Injection-moulding challenges: despite rheometric measurements showing lower compound viscosity with increasing slag content, injection moulding trials revealed significant flow limitations with coarse EAF slag particles (up to 100 μm) obstructing narrow mould gates (≈50 μm). Nevertheless, the processability of these compounds can be substantially improved through targeted mould design modifications (e.g., reduced cavity count, enlarged runner cross-sections, and optimized gate geometry) or by adopting alternative technologies. Conventional compression moulding—already validated at laboratory scale—offers a straightforward, low-shear route that ensures reliable filling, homogeneous dispersion, and consistent part quality across all slag content.
- Mechanical performance trade-offs: progressive reduction in mechanical properties occurred with increasing slag content, particularly in tear strength due to the angular geometry of slag particles.
- Increased wear rates: the abrasive nature of slag particles led to higher wear rates, potentially compromising long-term durability in some applications.

Overall, the 50 % slag substitution emerges as the most practical compromise between sustainability goals and performance requirements. Future work should focus on optimizing slag particle size distribution through finer grinding processes. From an industrial perspective, although achieving a slag granulometry below 100 μm through multi-stage crushing and milling would introduce an additional processing cost on the order of 30–40 € per ton [7], this value remains significantly lower than the typical bulk cost of conventional fillers such as carbon black (several hundred to over 1000 € per ton [31]). At the same time, the use of slag avoids slag disposal fees (40–80 € per ton) and supports circular-economy strategies through waste valorization.This research contributes to advancing sustainable material solutions in industrial elastomeric applications by providing a comprehensive assessment of both the technical feasibility and practical limitations of incorporating EAF slag as a functional filler in rubber compounds.

CRediT authorship contribution statement

Giorgio Ramorino: Writing – review & editing, Supervision, Project administration, Funding acquisition, Data curation, Conceptualization. **Maurício Azevedo:** Validation, Methodology, Investigation, Formal

analysis. **Roman Christopher Kerschbaumer:** Validation, Methodology, Investigation, Formal analysis. **Mario Costardi:** Formal analysis. **Mattia Ramini:** Validation, Resources, Investigation, Formal analysis. **Candida Petrogalli:** Investigation, Formal analysis. **Silvia Agnelli:** Writing – review & editing, Resources. **Giovanna Cornacchia:** Writing – review & editing, Validation, Supervision, Project administration, Methodology, Funding acquisition. **Anna Gobetti:** Writing – original draft, Methodology, Formal analysis, Data curation, Conceptualization.

Declaration of Generative AI and AI-assisted technologies in the writing process

During the preparation of this work the authors used ChatGPT and Claude AI in order to improve the readability and language of the manuscript. After using this tool/service, the authors reviewed and edited the content as needed and take full responsibility for the content of the published article.

Declaration of Competing Interest

The authors declare that they have no known competing financial interests or personal relationships that could have appeared to influence the work reported in this paper.

Acknowledgements

This work has been supported by Fondazione Cariplo, grant n◦ 2024–0654.The authors thank Ligom Spa for compounding the materials, Asonext Spa for providing the EAF slag and test equipment, and Italian Gasket for the industrial trials.

Appendix A. Supporting information

Supplementary data associated with this article can be found in the online version at doi:10.1016/j.jece.2026.121283.

Data Availability

No data was used for the research described in the article.

References

[1] F. Rosner, T. Bhagde, D.S. Slaughter, V. Zorba, J. Stokes-Draut, Techno-economic and carbon dioxide emission assessment of carbon black production, J. Clean. Prod. 436 (2024), https://doi.org/10.1016/j.jclepro.2023.140224.
[2] J. Suer, F. Ahrenhold, M. Traverso, Carbon footprint and energy transformation analysis of steel produced via a direct reduction plant with an integrated electric melting unit, J. Sustain. Met. 8 (2022), https://doi.org/10.1007/s40831-022-00585-x.
[3] N.M. Piatak, M.B. Parsons, R.R. Seal, Characteristics and environmental aspects of slag: a review, Appl. Geochem. 57 (2015) 236–266, https://doi.org/10.1016/j.apgeochem.2014.04.009.
[4] Federacciai, Relazione Annuale 2021, 2021. https://federacciai.it/pubblicazioni-varie/.
[5] I.Z. Yildirim, M. Prezzi, Chemical, mineralogical, and morphological properties of steel slag, Adv. Civ. Eng. 2011 (2011), https://doi.org/10.1155/2011/463638.
[6] A. Gobetti, G. Cornacchia, G. Tomasoni, K. Dey, G. Ramorino, Steel slag as a low-impact filler in rubber compounds for environmental sustainability, Mater. Manuf. Process 39 (2024) 1830–1841, https://doi.org/10.1080/10426914.2024.2334696.
[7] A. Gobetti, G. Cornacchia, G. Tomasoni, G. Ramorino, The Environmental Benefits of Industrial Symbiosis: A Case Study on Substituting Sand with Steel Slag as Filler in Epoxy Mortar, Waste Manag. Res. J. a Sustain. Circ. Econ. (2025), https://doi.org/10.1177/0734242X251350543.
[8] A. Gobetti, G. Cornacchia, M. Gelfi, G. Ramorino, White steel slag from ladle furnace as calcium carbonate replacement for nitrile butadiene rubber: a possible industrial symbiosis, Results Eng. 18 (2023) 101229, https://doi.org/10.1016/j.rineng.2023.101229.
[9] A. Gobetti, G. Cornacchia, S. Agnelli, M. Ramini, G. Ramorino, A novel and sustainable rubber composite prepared from electric arc furnace slag as carbon black replacement, Carbon Resour. Convers. 7 (2024), https://doi.org/10.1016/j.crcon.2024.100230.
[10] X. Ren, K. Cornish, Waste Conversion Into Sustainable and Reinforcing Fillers for Rubber Composites, Elsevier Ltd, 2020, https://doi.org/10.1016/b978-0-12-803581-8.10547-8.
[11] G.R. Martín-Cortés, F.J. Esper, A.J.Santana de Araujo, W.T. Hennies, M.G. Silva Valenzuela, F.R. Valenzuela-Díaz, Replacement of carbon black on natural rubber composites and nanocomposites - part 1, in: Charact. Miner. Met. Mater, 2016, Springer International Publishing, 2015, pp. 145–152, https://doi.org/10.1007/978-3-319-48191-3_18.
[12] P. Yuvaraj, J.R. Rao, N.N. Fathima, N. Natchimuthu, R. Mohan, Complete replacement of carbon black filler in rubber sole with CaO embedded activated carbon derived from tannery solid waste, J. Clean. Prod. 170 (2018) 446–450, https://doi.org/10.1016/j.jclepro.2017.09.188.
[13] C. Li, F. Huang, J. Wang, X. Liang, S. Huang, J. Gu, Effects of partial replacement of carbon black with nanocrystalline cellulose on properties of natural rubber nanocomposites, J. Polym. Eng. 38 (2018) 137–146, https://doi.org/10.1515/polyeng-2016-0382.
[14] D. Bosch, J.O. Back, D. Gurtner, S. Giberti, A. Hofmann, A. Bockreis, Alternative feedstock for the production of activated carbon with ZnCl<inf>2</inf>: Forestry residue biomass and waste wood, Carbon Resour. Convers. 5 (2022) 299–309, https://doi.org/10.1016/j.crcon.2022.09.001.
[15] P.J. Halley, M.E. Mackay, Chemorheology of thermosets - an overview, Polym. Eng. Sci. 36 (1996), https://doi.org/10.1002/pen.10447.
[16] ASTM, ASTM D297 Chemical Analysis Test Procedures for Rubber Products, Am. Soc. Test. Mater. (2021).
[17] R.C. Kerschbaumer, S. Stieger, M. Gschwandl, T. Hutterer, M. Fasching, B. Lechner, L. Meinhart, J. Hildenbrandt, B. Schrittesser, P.F. Fuchs, G.R. Berger, W. Friesenbichler, Comparison of steady-state and transient thermal conductivity testing methods using different industrial rubber compounds, Polym. Test. 80 (2019), https://doi.org/10.1016/j.polymertesting.2019.106121.
[18] ASTM E1530, Standard Test Method for Evaluating the Resistance to Thermal Transmission by the Guarded Heat Flow Meter Technique, (2019).
[19] ASTM D 624, Standard Test Method for Tear Strength of Conventional Vulcanized Rubber and, Annu. B. ASTM Stand. 00 (2012).
[20] n. 115 Ministero della tutela dell'ambiente e del territorio Gazzetta Ufficiale 19 maggio 2006, Individuazione dei rifiuti non pericolosi sottoposti alle procedure semplificate di recupero, ai sensi degli articoli 31 e 33 del decreto legislativo 5 febbraio 1997, n. 22, Italia, n.d.
[21] n. 201 Ministero della tutela dell'ambiente e del territorio Gazzetta Ufficiale del 30 agosto 2005, Definizione dei criteri di ammissibilità dei rifiuti in discarica, Italia, n. d.
[22] S. Zhang, R. Zhong, R. Hong, D. Hui, On factors affecting surface free energy of carbon black for reinforcing rubber, Nanotechnol. Rev. 9 (2020), https://doi.org/10.1515/ntrev-2020-0015.
[23] A.Y. Coran, Vulcanization: Conventional and Dynamic, Rubber Chem. Technol. 68 (1995), https://doi.org/10.5254/1.3538748.
[24] C.F.S. Gabriel, F.N. Linhares, A.M.F. De Sousa, C.R.G. Furtado, A.C.C. Peres, Vulcanization kinetic study of different nitrile rubber (NBR) compounds, Macromol. Symp. 344 (2014), https://doi.org/10.1002/masy.201300209.
[25] W.P. Cox, E.H. Merz, Correlation of dynamic and steady flow viscosities, J. Polym. Sci. 28 (1958), https://doi.org/10.1002/pol.1958.1202811812.
[26] M. Fasching, Robust Processing in Rubber Injection Molding Using Advanced Simulation Methods and Material Data, Montanuniversität Leoben, 2015.
[27] M. Ramini, S. Agnelli, Monitoring of shear heating effects during injection molding of rubber to improve the process control, Polym. Bull. 80 (2023), https://doi.org/10.1007/s00289-022-04376-y.
[28] J. Zhao, R. Yang, R. Iervolino, S. Barbera, Investigation of crosslinking in the thermooxidative aging of nitrile-butadiene rubber, J. Appl. Polym. Sci. (2015), https://doi.org/10.1002/app.41319.
[29] X. Liu, C. Fu, F. Wang, Y. Fang, G. Tang, D. Deng, K. Dai, Flame-retardant rigid polyurethane foam composites based on piperazine pyrophosphate/steel slag: a new strategy for utilizing metallurgical solid waste, J. Appl. Polym. Sci. (2025), https://doi.org/10.1002/app.56679.
[30] M. xue Shen, J. peng Zheng, X. kai Meng, X. Li, X. dong Peng, Influence of Al2O3 particles on the friction and wear behaviors of nitrile rubber against 316L stainless steel, J. Zhejiang Univ. Sci. A 16 (2015), https://doi.org/10.1631/jzus.A1400217.
[31] G. Wypych, Handbook of Fillers: Fourth Edition, 2016. https://doi.org/10.1016/C2015-0-01953-0.